

Monte Carlo simulations of the solid-liquid transition in hard spheres and colloid-polymer mixtures

T. Zykova-Timan¹, J. Horbach², and K. Binder¹

¹*Institut für Physik, Johannes Gutenberg-Universität Mainz, Staudinger Weg 7, 55099 Mainz, Germany*

²*Institut für Materialphysik im Weltraum, Deutsches Zentrum für Luft- und Raumfahrt (DLR), 51170 Köln, Germany*

(Dated: October 1, 2018)

Monte Carlo simulations at constant pressure are performed to study coexistence and interfacial properties of the liquid-solid transition in hard spheres and in colloid-polymer mixtures. The latter system is described as a one-component Asakura-Oosawa (AO) model where the polymer's degrees of freedom are incorporated via an attractive part in the effective potential for the colloid-colloid interactions. For the considered AO model, the polymer reservoir packing fraction is $\eta_p^r = 0.1$ and the colloid-polymer size ratio is $q \equiv \sigma_p/\sigma = 0.15$ (with σ_p and σ the diameter of polymers and colloids, respectively). Inhomogeneous solid-liquid systems are prepared by placing the solid fcc phase in the middle of a rectangular simulation box creating two interfaces with the adjoined bulk liquid. By analyzing the growth of the crystalline region at various pressures and for different system sizes, the coexistence pressure p_{co} is obtained, yielding $p_{co} = 11.576 \frac{k_B T}{\sigma^3}$ for the hard sphere system and $p_{co} = 8.0 \frac{k_B T}{\sigma^3}$ for the AO model (with k_B the Boltzmann constant and T the temperature). Several order parameters are introduced to distinguish between solid and liquid phases and to describe the interfacial properties. From the capillary-wave broadening of the solid-liquid interface, the interfacial stiffness is obtained for the (100) crystalline plane, giving the values $\tilde{\gamma} \approx 0.49 \frac{k_B T}{\sigma^2}$ for the hard-sphere system and $\tilde{\gamma} \approx 0.95 \frac{k_B T}{\sigma^2}$ for the AO model.

PACS numbers:

I. INTRODUCTION

Various colloidal systems are ideal models for the investigation of crystal nucleation and crystal growth processes. Whereas in atomistic systems, nucleation rates or interfacial free energies are hardly experimentally accessible from direct measurements, in colloidal systems the much larger length and time scales allow to determine these properties, at least in principle. For instance, *in situ* measurements of static structure factors in hard sphere-like colloidal systems using light scattering techniques resulted in estimates of nucleation rates and have given insight into the applicability of classical nucleation theory¹⁻³. Moreover, confocal microscopy gives a direct access to particle trajectories and thus, similar as in a computer simulation, any quantity of interest can be computed from the positions of the particles. Recently, several experimental studies using confocal microscopy⁴⁻⁷ have revealed various properties of solid-liquid interfaces. However, a direct estimate of anisotropic interfacial free energies in colloidal systems has not been possible so far.

Two paradigms of colloidal model systems that can be realized experimentally are hard spheres and hard spheres with a short-ranged attractive interaction (colloid-polymer mixtures). Due to the short-range of the interactions, these model systems are also well-suited for theoretical studies (e.g. in the framework of density functional theory^{8,9}) and for computer simulations. As far as the solid-fluid transition in hard spheres is concerned, various Molecular Dynamics (MD) and Monte Carlo (MC) techniques have been used to estimate thermodynamic properties such as the coexis-

tence pressure¹⁰⁻¹⁴, kinetic growth coefficients¹⁵, and interfacial free energies¹⁶⁻¹⁸. For the Asakura-Oosawa (AO) model of colloid-polymer mixtures (see below), MC studies^{19,20} have provided estimates for the solid-liquid phase boundaries in a wide range of model parameters. However, to our knowledge, interfacial free energies for solid-fluid interfaces have not been determined so far for the AO model.

Despite the efforts that have been recently undertaken, the examination of solid-liquid interfaces even for hard-sphere and hard-sphere-like systems is still subject to various problems. In particular, the role of finite-size effects has not been investigated in a systematic manner. Recently¹⁸, we have made a first preliminary step to fill this gap considering the solid-liquid interfaces of hard spheres and of the metallic system Ni. In the latter work, we have estimated the coexistence pressure and the interfacial stiffness $\tilde{\gamma}$ (see below) using constant-pressure MC simulations of solid-liquid inhomogeneous systems. To estimate $\tilde{\gamma}$, a result of capillary wave theory (CWT) was employed, according to which for a rough interface the mean-squared width of the interface grows logarithmically with the lateral size of the system. Thus, we have made use of finite-size effects to compute the interfacial stiffness $\tilde{\gamma}$.

In the present work, much more extensive calculations are performed to determine the coexistence pressure and various interfacial properties. In addition to the hard-sphere system, the AO model for colloid-polymer mixtures is considered. As a matter of fact, it is much more difficult to compute interfacial properties for the latter colloid-polymer model than for the hard sphere system due to a slower growth kinetics as well as

smaller-amplitude capillary fluctuations along the interface. However, we show that both for the hard sphere system and the AO model accurate values for the coexistence pressure are obtained without the requirement of extrapolation from relatively small system sizes to the thermodynamic limit.

The rest of the paper is organized as follows. In the next section the interaction models are introduced and the main details of the simulation are given. The results on the solid-fluid coexistence pressure are worked out in Sec. III A, followed by the introduction of local order parameters and the discussion of the interfacial structure in Sec. III B. Then, Sec. III C is devoted to the determination of the interfacial stiffness from the finite-size broadening of the interface. Finally, a summary and discussion of the results is provided in Sec. IV.

II. MODEL SYSTEMS AND SIMULATION TECHNIQUES

The one-component hard sphere model can be considered as the simplest model with a solid-liquid transition. For a system of hard spheres of diameter σ , the interaction potential is defined by

$$V_{\text{HS}}(r) = \begin{cases} \infty & r < \sigma \\ 0 & r \geq \sigma, \end{cases} \quad (1)$$

with r the distance between two particles. The freezing of hard spheres has been first observed in early molecular dynamics simulations^{21–23}. In these simulations, systems of $N = 500$ particles were considered. In this work, systems of up to 10^5 particles are investigated; in particular to obtain a reliable estimate of the interfacial stiffness $\tilde{\gamma}$.

To a very good approximation, the equation of state for the fluid phase of the hard sphere model is given by the analytical Carnahan-Starling equation^{24,25} and to a lesser degree for the solid by the Hall equation²⁶. Accurate values for the thermodynamic properties of the bulk solid are provided by empirical fits to computer simulations²⁷. Since any allowed hard-sphere configuration has zero potential energy, the solid-fluid transition in the hard-sphere system is completely driven by entropy and temperature T plays the role of a scaling factor. As a result, the thermodynamic properties are fully controlled by the packing density $\eta = \frac{\pi\sigma^3}{6} \frac{N}{V}$ (or, by the pressure p in case of fluctuating total volume V). At first glance, it seems to be surprising that hard spheres solidify since one may expect the entropy of an ordered solid phase to be always lower than that of the disordered fluid phase. However, at sufficiently high packing fractions, the spheres in a solid fcc configuration have locally more freedom to move than in a fluid at the same packing fraction, and the resulting higher number of possible microstates for the solid phase corresponds to a higher entropy.

Experimentally, the repulsive interactions between hard sphere colloids can be modified by the addition of

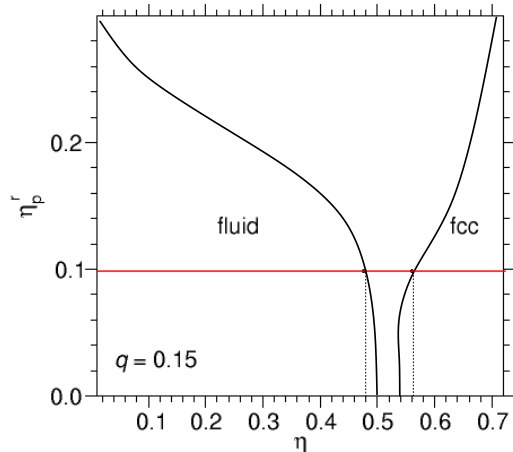


FIG. 1: A sketch of the phase diagram for the colloid-polymer mixture in the $\eta_p^r - \eta$ plane, assuming a polymer-colloid size ratio $q = 0.15$. Throughout this work, we consider either $\eta_p^r = 0.0$ (hard sphere model) or $\eta_p^r = 0.1$ (marked by the horizontal line).

non-adsorbing polymers. Although the pairwise colloid-polymer as well as the polymer-polymer interactions are repulsive, an effective attraction between the colloids in colloid-polymer mixtures is induced entropically by a depletion effect^{28,29}.

A simple model for colloid-polymer mixtures is the Asakura-Oosawa (AO) model^{30–32} where a hard sphere interaction is assumed between colloids as well as between colloids and polymers while polymer particles do not interact with each other. The limits of this approximation are discussed elsewhere^{33,34}. In this two-component model, the strength of the attractive interactions between the colloids is controlled by the density of polymer particles and the range of attraction by the size ratio between polymers and colloids, $q \equiv \sigma_p/\sigma$ (with σ_p and σ corresponding to the diameter of polymers and colloids, respectively). If one considers the system to be coupled to a polymer reservoir, the fugacity of polymers z_p (or the polymer reservoir packing fraction $\eta_p^r \equiv \frac{\pi\sigma_p^3 z_p}{6}$) can be regarded as the analog of inverse temperature in a molecular system and the phase diagram can be displayed in the $\eta_p^r - \eta$ plane (corresponding to the temperature-density plane in a molecular system). At $\eta_p^r = 0$ the coexistence region reduces to the case of pure hard spheres, whereas the increase of the polymer fugacity z_p broadens the coexistence region, corresponding to a higher coexistence packing fraction of the solid phase and a lower one of the fluid phase (Fig. 1). Note that throughout this work the polymer reservoir packing fraction is fixed at $\eta_p^r = 0.1$, as indicated by the horizontal line in Fig. 1.

On a qualitative level the AO model provides a good description of a colloid-polymer mixture. Modifications

of this model that lead to a more reliable description have been proposed elsewhere^{33,35–37}. On the other hand, the AO model can be simplified in terms of the computational load by integrating out the polymers degrees of freedom and represent the colloid-polymer mixture as a one-component system of colloidal particles that interact with each other via an effective interaction potential. While for $q \geq 0.154$, this potential is a sum of two-body, three-body and higher-body terms, for $q < 0.154$ it reduces to a pair potential given by^{30,31,38}

$$\beta V_{\text{AO}}(r) = \begin{cases} -\eta_p^r \frac{(1+q)^3}{q^3} \times \\ \left(1 - \frac{3r/\sigma}{2(1+q)} + \frac{(r/\sigma)^3}{2(1+q)^3}\right) & \sigma < r < \sigma + \sigma_p \\ 0 & r > \sigma + \sigma_p \end{cases} \quad (2)$$

with r the distance between two colloids and $\beta \equiv (k_B T)^{-1}$ (with k_B the Boltzmann constant).

In this work, the fluid-to-solid transition of the hard sphere system and the AO model, as described by the potential (2), is studied using Monte Carlo (MC) simulations in the isothermal-isobaric NpT and Np_zT ensembles, i.e. at constant pressure p , temperature T and particle number N (in the Np_zT ensemble, p_z is the diagonal component of the pressure tensor perpendicular to the xy plane, i.e. perpendicular to the interface). MC simulations were carried out using a standard Metropolis algorithm. The trial moves were particle displacements and a rescaling of the volume for one MC cycle^{39–41}. The maximum particle displacement was chosen such that the acceptance rate maintained constant at 30% for particle displacements and at 10% for volume's rescaling. To optimize the speed of the simulation for large system sizes, a cell-linked neighbor list was used^{40,41}.

III. RESULTS

A. Coexistence pressure

As a prerequisite for the investigation of interfacial properties, an accurate determination of the coexistence pressure p_{co} is required. To this end, inhomogeneous systems are prepared where the crystal phase in the middle of an elongated simulation box is surrounded by the fluid phase, separated by two planar interfaces (note that two interfaces appear due to the use of periodic boundary conditions). When solid and liquid are in equilibrium at the pressure p_{co} , the thermodynamic driving force is zero and the average total volume $\langle V(t) \rangle$ of the system does not change as a function of time, i.e. the crystal neither grows nor melts. In this manner, p_{co} can be identified as the pressure where the time derivative $\langle dV(t)/dt \rangle$ vanishes.

To prepare an inhomogeneous system at a given pressure, one has to first compute separately the equation of state, $p(\eta)$, for the pure fluid and the pure crystal. From the fluid and the solid branch of $p(\eta)$ one can then read

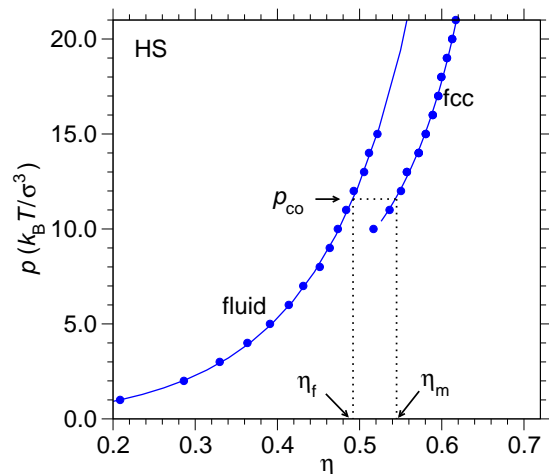


FIG. 2: Phase diagram of the hard sphere system in the (p, η) plane. The filled circles are simulation results, whereas the solid lines correspond to analytical expressions estimates of the equation of state, as proposed by Carnahan and Starling (fluid branch) and by Hall (solid branch). $p_{\text{co}} \approx 11.576$ is the estimated coexistence pressure at which the transition from a fluid to a crystalline fcc phase occurs. The coexistence region is between the freezing point at $\eta_f \approx 0.492$ and the melting point at $\eta_m \approx 0.545$.

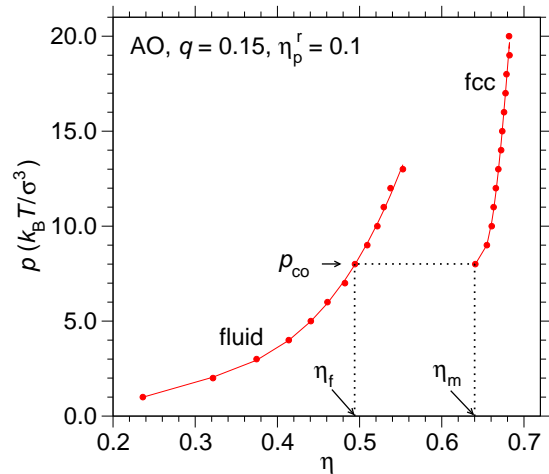


FIG. 3: Phase diagram of the AO model in the (p, η) plane for $q = 0.15$ and $\eta_p^r = 0.1$. The filled circles are the simulation results. Here, the solid lines are spline interpolations between simulation points. The estimated coexistence pressure is $p_{\text{co}} \approx 8.0$. Freezing and melting points are at $\eta_f \approx 0.494$ and $\eta_m \approx 0.64$, respectively.

off the packing fraction η (or the volume V) of the two phases at a given pressure. For the calculation of $p(\eta)$, we used MC simulations in the NpT ensemble. These runs were done for systems of $N = 500$ and, in some cases, for $N = 1728$ particles. The simulations with the larger system size indicated that finite-size effects are negligible for the calculation of the equation of state, at least for

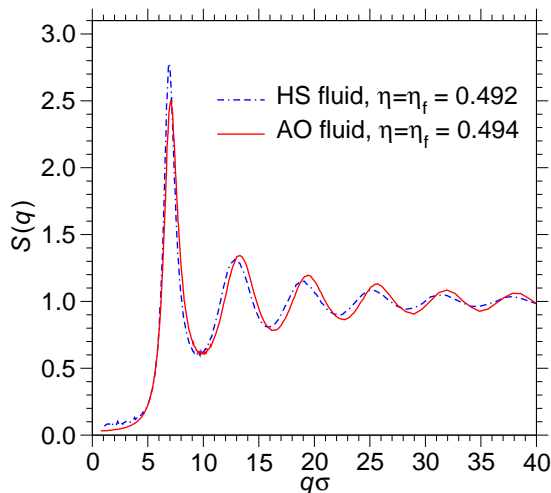


FIG. 4: Static structure factors $S(q)$ of the hard sphere and the AO fluid at the freezing point.

systems with $N \geq 500$ particles. The simulation time was chosen depending on the convergence of the results, ranging from 500000 to several million MC cycles.

Figures 2 and 3 display respectively the equation of state of the hard sphere and the AO systems (with $q = 0.15$ and $\eta_p^r = 0.1$). For the hard sphere system, the simulation results are well-described by analytical expressions (solid lines), as proposed by Carnahan and Starling²⁵ for the liquid branch and by Hall²⁶ for the fcc phase. In the case of the AO system, no accurate analytical predictions are available and so the solid lines in Fig. 3 are just spline interpolations that connect the data points. Also indicated in Figs. 2 and 3 are the coexistence pressure p_{co} and the corresponding packing fractions at freezing and melting, $\eta = \eta_f$ and $\eta = \eta_m$, respectively, as obtained from our MC simulations (see below). For the AO model, the coexistence region is much broader than for the hard sphere system. However, the freezing point is at a similar packing fraction around $\eta \approx 0.493$ for both models. Also the fluid structure at the freezing point is quite similar for the two systems. This can be inferred from Fig. 4 where the static structure factor²⁴ $S(q)$ is displayed for the hard sphere and the AO system at $\eta = \eta_f$. From these findings different properties of the solid-fluid interface may be expected for the AO system when compared to the hard spheres. While at coexistence the fluid structure and fluid density are very similar for both model systems, in the AO model the fluid coexists with a fcc crystal with a much higher packing density ($\eta_m \approx 0.64$) than in the hard sphere case where $\eta_m \approx 0.545$. Below we see that indeed the interfacial stiffness for the AO system is about a factor of 2 higher than that of the hard spheres.

Having computed the equations of state for the fluid and the solid phases, we now switch to the simulations of the inhomogeneous systems. As described above, the

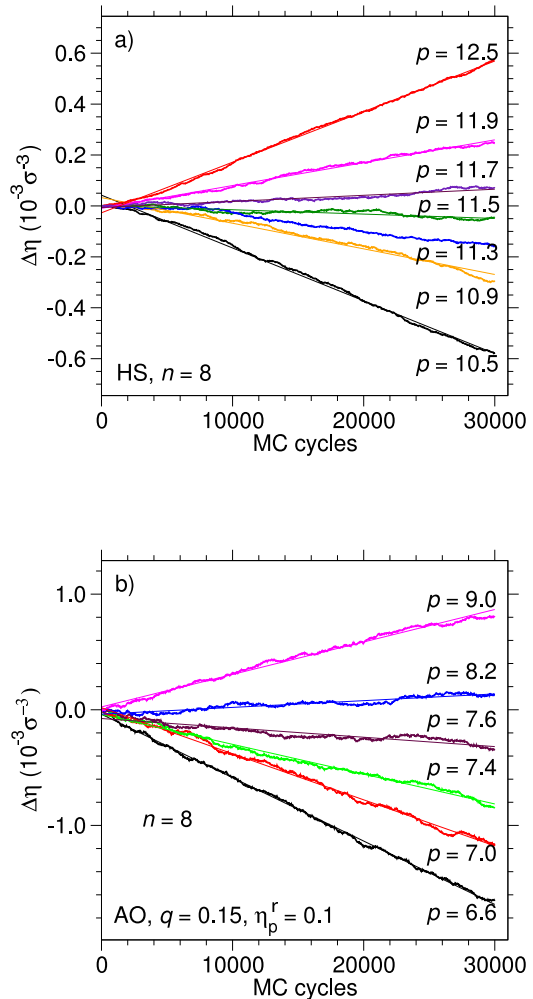


FIG. 5: The relative change of colloidal packing fraction, $\Delta\eta$, as a function of Monte Carlo cycles for different pressures, as indicated. The solid lines are fits from which $\langle dV/dt \rangle$ is determined. a) Hard sphere system, b) AO model with $q = 0.15$ and $\eta_p^r = 0.1$. In both cases, systems with $N = 10240$ particles are considered (corresponding to $n = 8$).

coexistence pressure p_{co} is obtained from the analysis of the change of the total volume as a function of time. The crystal grows or melts, dependent on the pressure at which the system is considered, and thus, the coexistence point is estimated as the state where the total volume of the system does not change with time. Despite the simplicity of this analysis, there are several pitfalls when applying this method. First, interactions between the interfaces due to periodic boundary conditions have to be eliminated. Therefore, we have done test runs with various ratios of L_z/L . As a result, $L_z = 5L$ was found to be an optimal choice for the avoidance of interaction effects between the interfaces. Second, finite-size effects

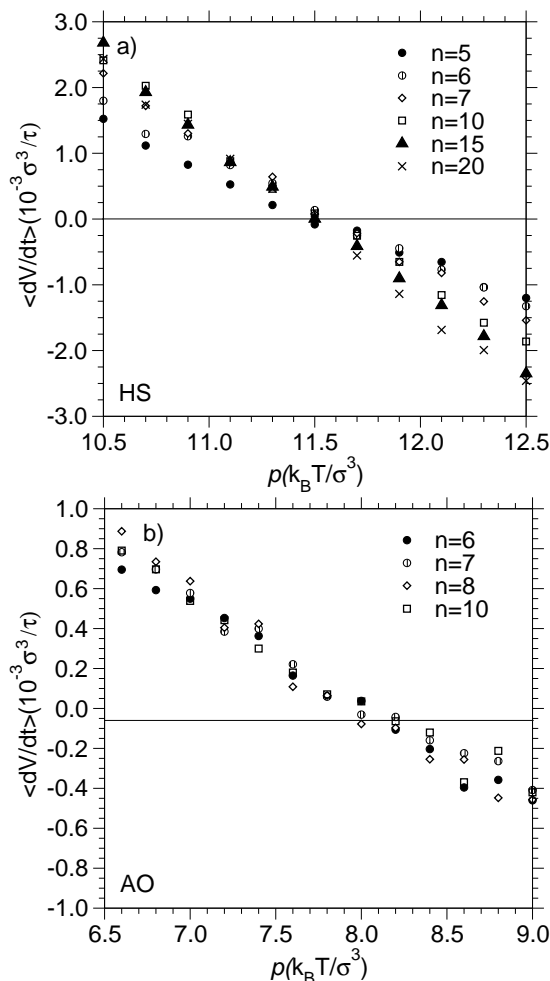


FIG. 6: Volume velocity $\langle dV/dt \rangle$ for different system sizes, as indicated. a) Hard sphere system, b) AO model.

need to be quantified to obtain reliable estimates of various properties at coexistence, such as the pressure or the interfacial stiffness. Therefore, we have considered various system sizes with $N = 2500, 4320, 6860, 10240, 20000, 67500,$ and 160000 particles. Third, the crystal-liquid interfaces have to be prepared such that no artificial strains are generated in the crystalline region. In particular, the use of the isotropic NpT ensemble is not appropriate for the simulation of solid-liquid coexistence. The uniform volume moves in NpT simulations lead inevitably to strains in the xy plane of the crystal, since the number of lattice planes cannot change in these moves. Thus, the lateral dimensions of the system need to be fixed such that they are commensurate with the chosen integer number of lattice planes (note that the lattice spacing at a given pressure is known from the bulk simulations of the pure fcc phase). Then, the volume is allowed to fluctuate in z direction (perpendicular to the interfaces), keeping the pressure in that direction (p_z) constant.

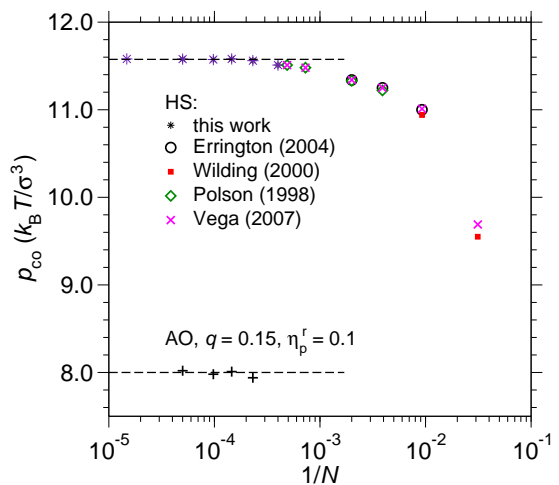


FIG. 7: Coexistence pressure as a function of system size (in terms of the inverse number of particles, $1/N$) for the hard sphere system and the AO model. The dashed lines indicate the estimated coexistence pressures in the thermodynamic limit, $p_{co} = 11.576$ for the hard sphere system and $p_{co} = 8.0$ for the AO model. For the hard sphere system, results of other studies are included (from Errington¹³, Wilding and Bruce¹², Polson and Frenkel¹¹, and Vega and Noya¹⁴).

To generate crystal-fluid samples at various pressures, first independent solid and fluid samples were simulated. The solid was put into a simulation box with dimensions $L \times L \times 3L$, thereby aligning the (100) plane of the fcc crystal perpendicular to the z -axis. The box length L was chosen such that it corresponds to the solid density at the considered pressure. At the same density, a starting configuration for the fluid was generated by putting the particles randomly in a box of size $L \times L \times 2L$. Then, the box dimensions of the fluid in x - and y -direction were kept fixed and the fluid was equilibrated by a MC simulation in the Np_zT ensemble. After 10^6 MC cycles, solid and fluid samples were sufficiently thermalized and put together into a simulation box of approximate size $L \times L \times 5L$ (applying periodic boundary conditions in all three spatial dimensions), followed by further simulations in the Np_zT ensemble. In the latter runs, the positions of the solid particles were fixed for the first 10^5 MC cycles to equilibrate the crystal-fluid interface without melting away the crystal due to an unfavorable local packing of particles in the interface region after matching the fluid slab with the solid slab. Then, the solid particles were released for the rest of the simulation. Finally, a set of short runs over 3×10^4 MC cycles were performed in a wide range of pressures to obtain at each pressure the total volume as a function of time.

As an example, Fig. 5 shows the relative change of the colloidal packing fraction, $\Delta\eta$, at different pressures for systems of 10240 particles. At this system size, the lateral dimension is given by $L = L_x = L_y = na$ with $n = 8$ lattice planes in units of the lattice constant a (of course,

a changes as a function of pressure both for the AO and the HS system). In the following, we indicate the system size in terms of the number n , considering box geometries of nominal size $L \times L \times 5L$. We also note that the time t is measured in units of the number of Monte Carlo cycles; of course, it cannot be directly translated into a physical time, but, since we are not interested in the growth kinetics here, this does not matter in the present context.

The slopes $\langle dV/dt \rangle$, averaged over 10 independent configurations, are displayed in Fig. 6 for different system sizes, ranging from $n = 5$ to $n = 20$ for the hard sphere system and from $n = 6$ to $n = 10$ for the AO system. The values for p_{co} , as estimated via the interpolation to $\langle dV/dt \rangle = 0$ for the different system sizes, are plotted in Fig. 7 as a function of the inverse number of particles $1/N$. Obviously, both for the HS and the AO model, finite-size effects are small in the considered range of system sizes and we obtain $p_{co} = 11.576 \pm 0.006 \frac{k_B T}{\sigma^3}$ for the hard spheres and $p_{co} = 8.0 \pm 0.026 \frac{k_B T}{\sigma^3}$ for the AO model. The corresponding packing fractions for freezing and melting are respectively given by $\eta_f = 0.492$ and $\eta_m = 0.545$ for the hard spheres and by $\eta_f = 0.494$ and $\eta_m = 0.64$ for the AO model (see also Figs. 2 and 3).

Also included in Fig. 7 are estimates of p_{co} for the hard sphere system, as obtained from other simulation studies^{11–14}. In these studies, the use of thermodynamic integration techniques as well as the phase switch MC method allowed only the consideration of relatively small system sizes and so these results lie below the dashed line in Fig. 7 that marks the estimate of p_{co} in the thermodynamic limit, as obtained from our simulation. This indicates the advantage of the methodology used in this work: relatively large system sizes can be simulated and thus it is not necessary to perform extrapolations to the thermodynamic limit (at least not for the systems considered here) that may easily lead to systematic errors in the estimate of the coexistence pressure.

B. Local order parameters and interfacial structure

Having determined p_{co} for the hard sphere and the AO model, we can now investigate properties of solid-fluid interfaces in these systems at coexistence. First, order parameters have to be identified that allow to distinguish between solid-like and fluid-like local order around a particle. A class of order parameters that is well-suited for this purpose are local bond order parameters, $Q_l(i)$, as introduced by Steinhardt *et al.*⁴². They are based on the expansion into spherical harmonics Y_{lm} :

$$Q_l(i) = \left(\frac{4\pi}{2l+1} \sum_{m=-l}^l |\bar{Q}_{lm}|^2 \right)^{1/2} \quad (3)$$

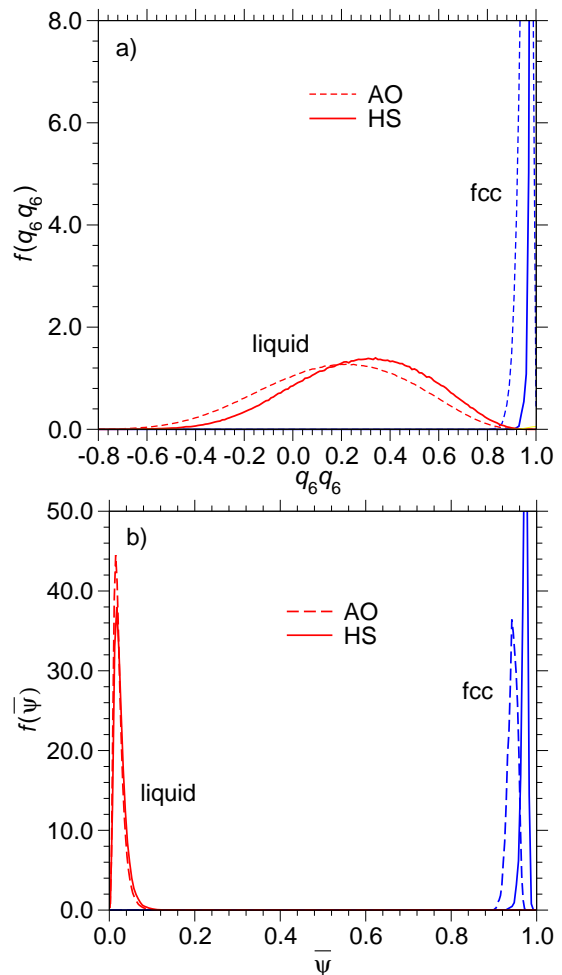


FIG. 8: Order parameter distributions for the AO model (dashed lines) and the hard sphere system (solid lines) for the liquid and the fcc phase, as indicated; a) $q_6 q_6$, b) $\bar{\Psi}$.

with

$$\bar{Q}_{lm}(i) = \frac{1}{Z_i} \sum_{j=1}^{Z_i} Y_{lm}(\theta(\vec{r}_{ij}), \phi(\vec{r}_{ij})), \quad (4)$$

where \vec{r}_{ij} is the distance vector between a pair of neighboring particles i and j , Z_i is the number of neighbors within a given cut-off radius, and $\theta(\vec{r}_{ij})$ and $\phi(\vec{r}_{ij})$ are the polar bond angles with respect to an arbitrary reference frame.

A variant of the order parameters (3) has been put forward by ten Wolde *et al.*⁴³ by introducing the dot product

$$q_l q_l(i) = \frac{1}{Z_i} \sum_{j=1}^{Z_i} \sum_{m=-l}^l \tilde{q}_{lm}(i) \tilde{q}_{lm}(j)^*, \quad (5)$$

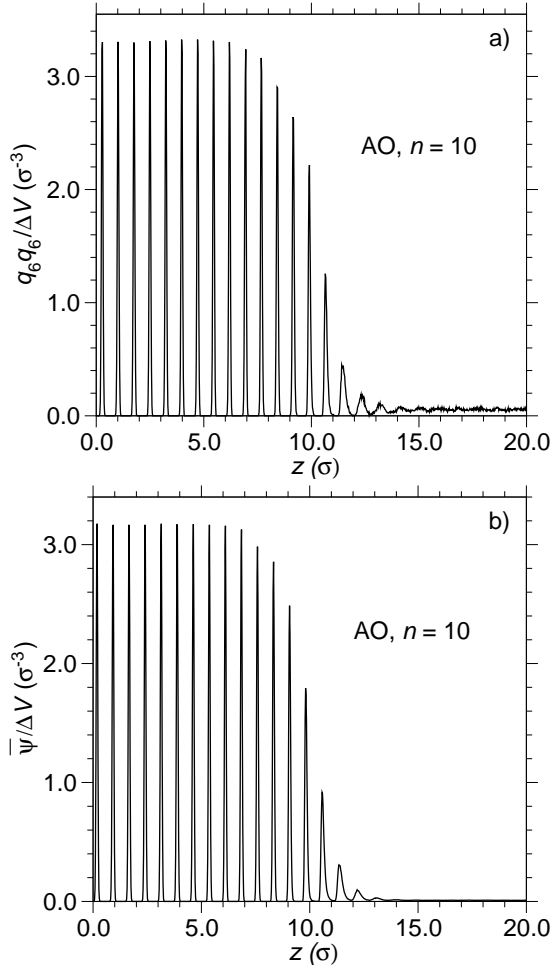


FIG. 9: Fine-grained order parameter profiles of a) q_6q_6 and b) $\bar{\Psi}$ for the AO model. The system contains 20000 particles, corresponding to $n = 10$.

with

$$\tilde{q}_{lm}(i) = \frac{\bar{Q}_{lm}(i)}{\left(\sum_{m=-l}^l |\bar{Q}_{lm}(i)|^2\right)^{1/2}}. \quad (6)$$

Here, we use q_6q_6 that is defined by Eqs. (5) and (6), setting $l = 6$.

Figure 8a shows the q_6q_6 distributions for the pure fluid and fcc phases at coexistence for the hard sphere system (solid lines) and the AO mixture (dashed lines). The relatively small overlap of the distribution for the solid with that of the fluid indicates that q_6q_6 is well-suited to distinguish between solid and fluid particles. Note that we have used time-averaged particle positions for the calculation of the order parameter distributions in Fig. 8a (also for the distributions shown in Fig. 8b). Particle positions were averaged over 50 MC cycles in case of the hard sphere system and over 20 MC cycles in case of the AO mixture. This reduces the shift of the order parameter distributions for the solid fcc phases to lower values

of the order parameter, as compared to the distribution of an ideal fcc crystal.

A different local order parameter has been introduced by Morris^{44,45}. It is defined by

$$\Psi(i) = \left| \frac{1}{N_q} \frac{1}{Z_i} \sum_{j=1}^{Z_i} \sum_{k=1}^{N_q} \exp(i\vec{q}_k \cdot \vec{r}_{ij}) \right|^2 \quad (7)$$

where \vec{r}_{ij} denotes the distance vector of a particle i to neighboring particles j , and the wave-vectors \vec{q}_k are related to reciprocal vectors of the fcc lattice with lattice constant a_0 , $\vec{q}_1 = 2\pi/a_0(-1, 1, -1)$, $\vec{q}_2 = 2\pi/a_0(1, -1, 1)$ and $\vec{q}_3 = 2\pi/a_0(1, 1, -1)$. An additional average of $\Psi(i)$ over a particle with index i and its neighboring particles in the first coordination shell yields

$$\bar{\Psi}(i) = \frac{1}{Z_i + 1} \left(\Psi(i) + \sum_{j=1}^{Z_i} \Psi(j) \right) \quad (8)$$

As can be inferred from Fig. 8b, the $\bar{\Psi}(i)$ distributions display a sharp peak close to $\bar{\Psi} = 1$ for the fcc phase and one close to $\bar{\Psi} = 0$ for the fluid. Obviously, the order parameter $\bar{\Psi}$ is also well-suited to identify the local order around particles.

By applying the methodology of our previous study¹⁸, we characterize the local structure of the interfaces by z -dependent profiles of averaged local order parameters. For this purpose solid-fluid samples were divided into bins of length $\Delta z = 0.05\sigma$ along the z -direction and "time" averages of the order parameter were obtained for each bin, thereby correcting for shifts of the crystal planes with respect to the reference frame during the simulation.

Figures 9a and 9b show order parameter profiles for the AO model as a function of the z -coordinate (i.e. perpendicular to the interface). To obtain these profiles, the sum of the order parameter of the particles in each bin transversal to the solid-fluid interface is divided by the volume of the bin $\Delta V = L^2\Delta z$. In the crystalline region, the profiles exhibit strong oscillations with the periodicity of the crystalline planes. The amplitude of these oscillations decay rapidly in the interfacial region and flatten completely in the fluid region. Corresponding data for the hard-sphere system are reported in our previous study¹⁸.

C. Finite-size interfacial broadening and interfacial stiffness

Now, we aim at computing the interfacial stiffness $\tilde{\gamma}$ which is defined by $\tilde{\gamma} = \gamma + d^2\gamma/d\theta^2$ with γ the interfacial tension and θ the angle between the interface normal and the (100) direction. Whereas γ describes the free energy cost to increase the area of the interface, the term $d^2\gamma/d\theta^2$ accounts for the free energy required to locally change the orientation of the crystal. The latter term

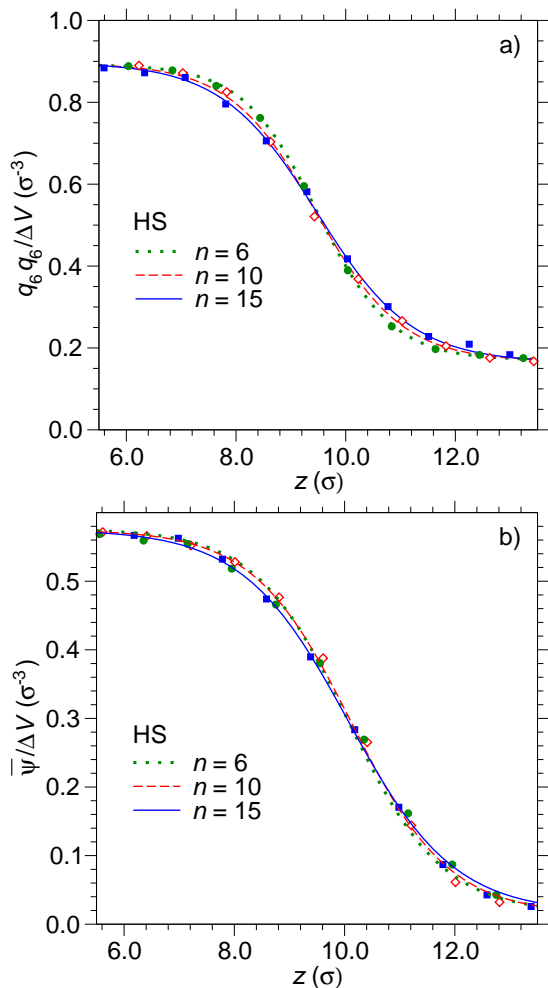


FIG. 10: Coarse-grained order parameter profiles for the hard sphere system for different system sizes; a) $q_6 q_6$, b) Ψ . The lines are fits to Eq. (9).

would of course vanish for a system where both phases at the interface are isotropic (as, e.g., in the case of liquid-gas interfaces).

In the framework of capillary wave theory (CWT), the interfacial stiffness can be computed from the broadening of the solid-fluid interface with increasing lateral size of the system¹⁸ (see below). To make use of this prediction, the apparent mean-squared width of the interface, w^2 , has to be determined and analyzed as a function of system size. For this purpose, fine-grid order profiles as the ones shown in Fig. 9 are not well-suited since the oscillations due to the crystalline order do not allow to fit the profile with a simple function where the interfacial width appears as a free parameter. Therefore, it is useful to coarse-grain the profiles by averaging over the oscillations. To this end, we have identified the minima in the fine-grid profiles and used them to mark the borders of non-uniform bins that match the crystalline layers. Then, we took the average of the order parameter in each of the

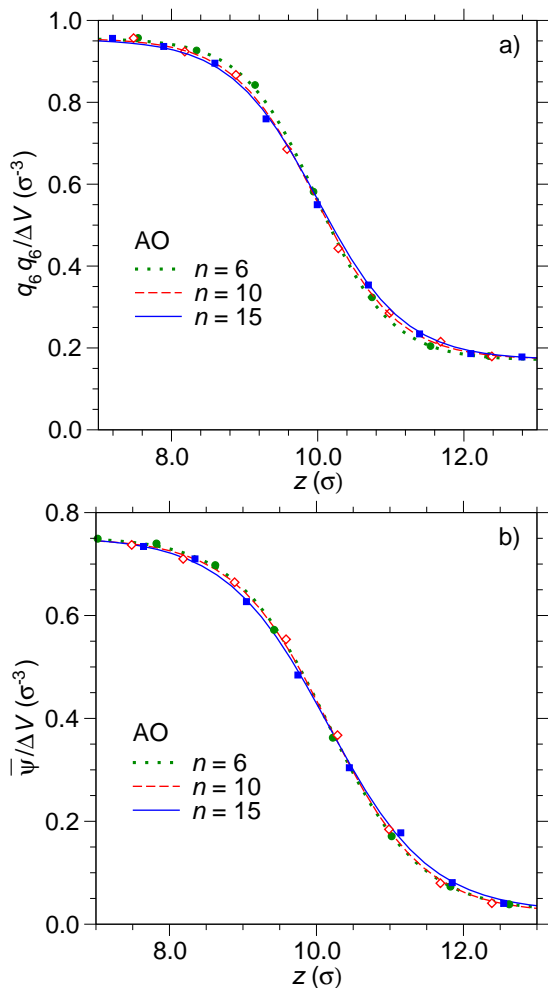


FIG. 11: Coarse-grained order parameter profiles for the AO model for different system sizes; a) $q_6 q_6$, b) Ψ . The lines are fits to Eq. (9).

latter bins.

Examples of the resulting coarse-grained profile for different system sizes are shown in Figs. 10 and 11. As we can see in these plots, the data can be well fitted with hyperbolic tangent function of the following form

$$\phi(z) = \frac{A+B}{2} + \frac{A-B}{2} \tanh\left(\frac{z-z_0}{w}\right) \quad (9)$$

where A and B are the bulk order parameters in the solid and fluid obtained from the independent bulk simulations. So the position of the interface z_0 and its width w are the only fit parameters. Note that Eq. (9) can be obtained in the framework of mean-field theory. However, here it is just used a fitting function to determine the width w as a function of the lateral size of the system. Figures 10 and 11 indicate that both for the hard sphere model and the AO mixture, w slightly increases with increasing system size.

The finding that the width w is system-size-dependent

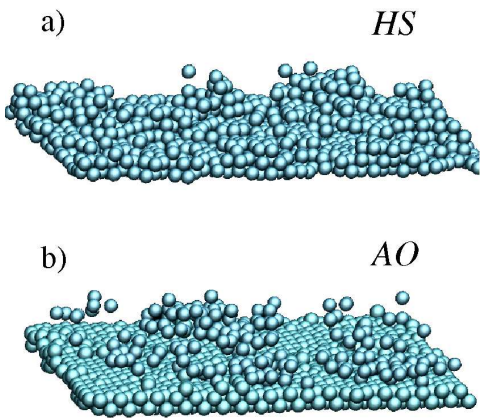


FIG. 12: Snapshots of the interfaces for a) hard spheres and b) the AO model for systems with $n = 15$. Here, only solid particles are shown, defining a particle as a solid one when its $q_6 q_6 > 0.6$ and its coordination number greater than 10.

is expected from CWT where the mean-squared interfacial width is found to diverge logarithmically with the lateral size L of the system^{46–49},

$$w^2 = w_0^2 + \frac{k_B T}{4\tilde{\gamma}} \ln \frac{L}{l}, \quad (10)$$

with w_0 the so-called intrinsic width and l a cut-off parameter that has to be introduced since CWT only describes long-wavelength undulations of the interface. Note that it is impossible to disentangle the intrinsic width contribution w_0^2 from the cut-off contribution $\frac{k_B T}{4\tilde{\gamma}} \ln l$. An extensive discussion of this issue has been provided for the case of polymer mixtures^{50–54}.

The existence of capillary waves is associated with the roughness of the interface and the applicability of CWT requires that interfaces above a possible roughening transition^{55–59} are considered. That both for the hard sphere system and the AO mixture the solid-fluid interface is indeed rough, is indicated by the snapshots in Fig. 12. Here, only the solid particles are shown, defining a particle as a solid one if $q_6 q_6 > 0.6$ and if its nearest-neighbor coordination number is larger than 10 (note that we have only needed this definition for the snapshots in Fig. 12). The snapshots reveal that the solid-fluid interface of the hard sphere system is significantly “more rough” than that of the AO mixture. This might be due to the larger density difference between the fcc and the fluid phase in case of the AO model, when compared to the hard sphere system.

In Fig. 13, the prediction (10) is confirmed: both for the hard spheres and the AO mixture, the mean-squared width w^2 exhibits a logarithmic divergence with respect to the lateral dimension L . Within the statistical errors, the two order parameters $q_6 q_6$ and $\bar{\Psi}$ yield similar results. From the fits with Eq. (10), we estimate for the (100)

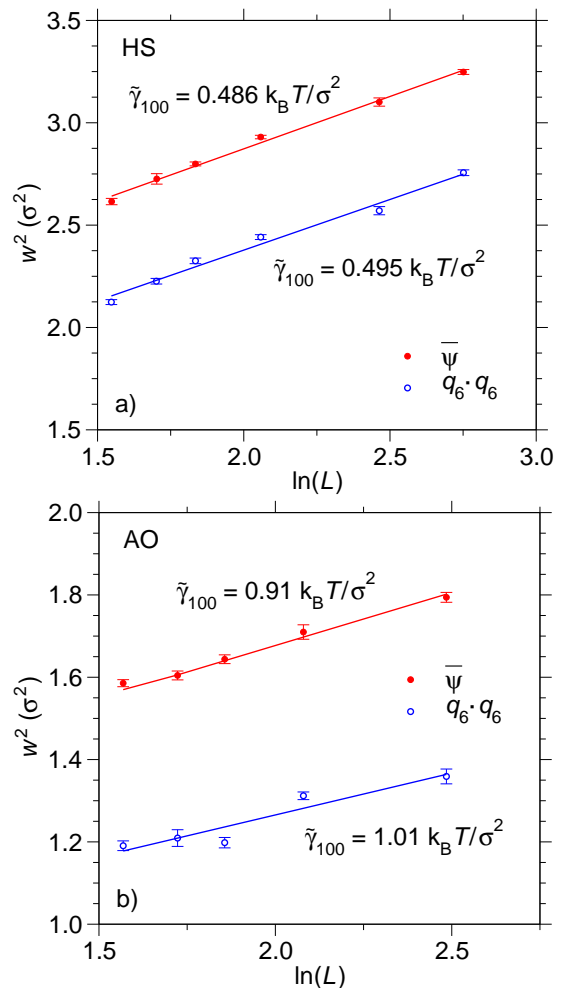


FIG. 13: Mean-squared width w^2 as a function of $\ln L$, for a) hard spheres and b) the AO model. The values for $\tilde{\gamma}$ are obtained from the fits (solid lines) to Eq. (10).

orientation $\tilde{\gamma} \approx 0.49 \pm 0.02 k_B T / \sigma^2$ for the hard sphere system and $\tilde{\gamma} \approx 0.95 \pm 0.1 k_B T / \sigma^2$ for the AO mixture. The value of $\tilde{\gamma}$ for the hard sphere system roughly agrees with previous estimates, obtained by other methods (for a discussion of this issue, see Refs.^{18,60}).

IV. CONCLUSIONS

We have investigated the fluid-to-crystal transition of two paradigmatic colloidal model systems using Monte Carlo (MC) simulations at constant pressure. Inhomogeneous systems have been prepared where the crystal phase in the middle of an elongated simulation box is separated from the fluid phase by two interfaces. We have demonstrated that MC simulations with this setup allow for reliable estimates of the coexistence pressure, p_{co} , and the interfacial stiffness, $\tilde{\gamma}$. Both for the hard sphere system and the AO mixture, our methodology al-

lows for the simulation of relatively large systems and thus, the coexistence pressure p_{co} can be computed without relying on error-prone extrapolations to the thermodynamic limit. On the other hand, we have presented a method for the calculation of $\tilde{\gamma}$ that makes use of finite-size effects due to the capillary-wave broadening of the interface. So far, this method has been mainly applied to polymer interfaces⁵¹, liquid-vapor interfaces⁶¹, isotropic-nematic interfaces⁶² or interfaces in Ising systems⁶³, but not to solid-fluid interfaces, as in this work (an exception is of course our recent preliminary work on hard spheres and nickel¹⁸). It requires a systematic variation of the system size and relatively small statistical errors to resolve the logarithmic divergence of the mean-squared interfacial width, as predicted in the framework of capillary wave theory (CWT). With respect to the latter issues, the determination of $\tilde{\gamma}$ is much more difficult for the AO mixture than for the hard sphere system. First, in the relevant range of colloid packing fractions η mass transport processes of the AO fluid in the bulk and in the interface region are much slower than in the hard sphere system. Therefore, much longer simulation runs are necessary for the AO model, to achieve comparable statistics as in the hard sphere system. Second, the interfacial stiffness $\tilde{\gamma}$ for the AO model is about a factor of two higher than in the hard sphere system, associated with lower-amplitude capillary fluctuations at comparable system sizes. Thus, the signal-to-noise ratio is worse for the AO model when one analyzes the interfacial fluctuations. However, despite the latter difficulties, the estimate of $\tilde{\gamma}$ from the

interfacial broadening works also well for the AO model.

CWT can be of course only applied to the analysis of interfacial properties, if rough, non-faceted interfaces are considered. Otherwise, there would be no divergence of the width of the interface with increasing lateral size of the system. For the case of the model systems considered in this work, the applicability of CWT is justified since we observe the logarithmic growth of the mean-squared interfacial width as a function of the lateral dimension L . To further rationalize the use of CWT, we plan to study the Fourier spectrum of interfacial fluctuations from which one can alternatively determine the interfacial stiffness. Moreover, we plan to investigate the possibility of a roughening transition of the AO model where the solid-fluid interface changes from a faceted to a rough interface with long-wavelength capillary wave fluctuations.

Acknowledgments

We thank Philipp Kuhn for a critical reading of the manuscript. We are grateful to the German Science Foundation (DFG) for financial support in the framework of the focus program SPP 1296. We acknowledge a substantial grant of computer time at the SOFT-COMP of the John von Neumann Institute for Computing (NIC) and the computer center (ZDV) of the Johannes Gutenberg-Universität Mainz.

-
- ¹ K. Schätzel and B. J. Ackerson, Phys. Rev. Lett. **68**, 337 (1992).
- ² J. L. Harland and W. van Meegen, Phys. Rev. E **55**, 3054 (1997).
- ³ H. J. Schöpe, G. Bryant, and W. van Meegen, Phys. Rev. Lett. **96**, 175701 (2006).
- ⁴ U. Gasser, E. R. Weeks, A. Schofield, P. N. Pusey, and D. A. Weitz, Science **292**, 258 (2001).
- ⁵ R. P. A. Dullens, D. G. A. L. Aarts, and W. K. Kegel, Phys. Rev. Lett. **97**, 228301 (2006).
- ⁶ V. Prasad, D. Semwogerere, and E. R. Weeks, J. Phys.: Condens. Matter **19**, 113102 (2007).
- ⁷ J. Hernández-Guzmán and E. R. Weeks, PNAS **106**, 15198 (2009).
- ⁸ W. A. Curtin, Phys. Rev. B **39**, 6775 (1988).
- ⁹ G. Kahl and H. Löwen, J. Phys.: Condens. Matter **21**, 464101 (2009).
- ¹⁰ D. Frenkel, J. Chem. Phys. **81**, 3188 (1984).
- ¹¹ J. M. Polson and D. Frenkel, J. Chem. Phys. **109**, 318 (1998).
- ¹² N. B. Wilding and A. D. Bruce, Phys. Rev. Lett. **85**, 5138 (2000).
- ¹³ J. R. Errington, J. Chem. Phys. **120**, 3130 (2004).
- ¹⁴ C. Vega and E. G. Noya, J. Chem. Phys. **127**, 154113 (2007).
- ¹⁵ M. Amini and B. B. Laird, Phys. Rev. Lett. **97**, 216102 (2006).
- ¹⁶ R. L. Davidchack and B. Laird, Phys. Rev. Lett. **85**, 4571 (2000).
- ¹⁷ R. L. Davidchack, J. R. Morris, and B. B. Laird, J. Chem. Phys. **125**, 094710 (2006).
- ¹⁸ T. Zykova-Timan, R. E. Rozas, J. Horbach, and K. Binder, J. Phys.: Condens. Matter **21**, 464102 (2009).
- ¹⁹ M. Dijkstra, J. M. Brader, and R. Evans, J. Phys.: Condens. Matter **11**, 10079 (1999).
- ²⁰ M. Dijkstra, R. van Roij, R. Roth, and A. Fortini, Phys. Rev. E **73**, 041404 (2006).
- ²¹ B. J. Alder and T. E. Wainwright, J. Chem. Phys. **27**, 1208 (1957).
- ²² W. G. Hoover and F. H. Ree, J. Chem. Phys. **49**, 3609 (1968).
- ²³ W. W. Wood and J. D. Jacobson, J. Chem. Phys. **27**, 1207 (1957).
- ²⁴ J. P. Hansen and I. R. McDonald, *Theory of simple liquids* (Academic Press, New York, 1986).
- ²⁵ N. F. Carnahan and K. E. Starling, J. Chem. Phys. **51**, 635 (1969).
- ²⁶ K. R. Hall, J. Chem. Phys. **57**, 2252 (1972).
- ²⁷ R. J. Speedy, Mol. Phys. **95**, 169 (1998).
- ²⁸ A. P. Gast, C. K. Hall, and W. B. Russel, J. Colloid Interf. Sci. **96**, 251 (1984).
- ²⁹ H. N. W. Lekkerkerker, W. C. K. Poon, P. N. Pusey, A. Stroobants, and P. Warren, Europhys. Lett. **20**, 559 (1992).

- ³⁰ S. Asakura and F. Oosawa, *J. Chem. Phys.* **22**, 1255 (1954).
- ³¹ S. Asakura and F. Oosawa, *J. Polym. Sci.* **23**, 183 (1958).
- ³² A. Vrij, *Pure Appl. Chem.* **48**, 471 (1976).
- ³³ E. J. Meijer and D. Frenkel, *J. Chem. Phys.* **100**, 6873 (1994).
- ³⁴ P. J. Flory, *Principles of Polymer Chemistry* (Cornell University Press, Ithaca and London, 1953).
- ³⁵ R. L. C. Vink, A. Jusufi, J. Dzubiella, and C. N. Likos, *Phys. Rev. E* **72**, 134905 (2005).
- ³⁶ J. Zausch, P. Virnau, J. Horbach, R. L. C. Vink, and K. Binder, *J. Chem. Phys.* **130**, 064906 (2009).
- ³⁷ J. Zausch, J. Horbach, P. Virnau, and K. Binder, *J. Phys.: Condens. Matter*, accepted for publication (2010).
- ³⁸ M. Dijkstra and R. van Roij, *Phys. Rev. Lett.* **89**, 208303 (2002).
- ³⁹ D. P. Landau and K. Binder, *A Guide to Monte Carlo Simulations in Statistical Physics* (Cambridge University Press, Cambridge, 2000).
- ⁴⁰ D. Frenkel and B. Smit, *Understanding Molecular Simulation* (Computational Science Series, 2002).
- ⁴¹ W. Krauth, *Statistical Mechanics: Algorithms and Computations* (Oxford University Press, Oxford, 2006).
- ⁴² P. J. Steinhardt, D. R. Nelson, and M. Ronchetti, *Phys. Rev. B* **28**, 784 (1983).
- ⁴³ P. R. T. Wolde, M. J. Ruiz-Montero, and D. Frenkel, *Phys. Rev. Lett.* **75**, 2714 (1995).
- ⁴⁴ J. R. Morris and X. Song, *J. Chem. Phys.* **116**, 9352 (2002).
- ⁴⁵ J. R. Morris, *Phys. Rev. B* **66**, 144104 (2002).
- ⁴⁶ F. P. Buff, R. A. Lovett, and F. H. Stillinger, *Phys. Rev. Lett.* **15**, 621 (1965).
- ⁴⁷ J. D. Weeks, *J. Chem. Phys.* **67**, 3106 (1977).
- ⁴⁸ D. Bedeaux and J. D. Weeks, *J. Chem. Phys.* **82**, 972 (1985).
- ⁴⁹ M. P. Gelfand and M. E. Fisher, *Physica A* **166**, 1 (1990).
- ⁵⁰ A. Werner, F. Schmid, M. Müller, and K. Binder, *J. Chem. Phys.* **107**, 8175 (1997).
- ⁵¹ A. Werner, F. Schmid, M. Müller, and K. Binder, *Phys. Rev. E* **59**, 728 (1999).
- ⁵² A. Werner, M. Müller, F. Schmid, and K. Binder, *J. Chem. Phys.* **110**, 1221 (1999).
- ⁵³ T. Kerle, J. Klein, and K. Binder, *Eur. Phys. J. B* **7**, 401 (1999).
- ⁵⁴ K. Binder and M. Müller, *Int. J. Mod. Phys. C* **11**, 1093 (2000).
- ⁵⁵ W. J. Shugard, J. D. Weeks, and G. H. Gilmer, *Phys. Rev. Lett.* **31**, 549 (1978).
- ⁵⁶ E. Burkner and D. Stuffer, *Z. Phys. B* **53**, 241 (1983).
- ⁵⁷ K. K. Mon, S. Wansleben, D. P. Landau, and K. Binder, *Phys. Rev. Lett.* **60**, 708 (1988).
- ⁵⁸ K. K. Mon, S. Wansleben, D. P. Landau, and K. Binder, *Phys. Rev. B* **39**, 7089 (1989).
- ⁵⁹ F. Schmid and K. Binder, *Phys. Rev. B* **46**, 13565 (1992).
- ⁶⁰ B. B. Laird and R. L. Davidchack, *J. Phys. Chem. B* **109**, 17802 (2005).
- ⁶¹ R. L. C. Vink, J. Horbach, and K. Binder, *J. Chem. Phys.* **122**, 134905 (2005).
- ⁶² S. Wolfsheimer, C. Tanase, K. Shundyak, R. van Roij, and T. Schilling, *Phys. Rev. E* **73**, 061703 (2006).
- ⁶³ M. Müller and G. Münster, *J. Stat. Phys.* **118**, 669 (2005).